Soft Matter

PAPER

View Article Online
View Journal | View Issue

Cite this: *Soft Matter*, 2020, **16**, 2753

Unravelling humidity-gated, temperature responsive bilayer actuators†

Rob C. P. Verpaalen,[ab] Anne E. J. Souren,[a] Michael G. Debije,[a] Tom A. P. Engels,[cb] Cees W. M. Bastiaansen[abd] and Albertus P. H. J. Schenning*[ab]

Received 6th January 2020,
Accepted 14th February 2020

DOI: 10.1039/d0sm00030b

rsc.li/soft-matter-journal

By spraying liquid crystal mixtures onto stretched polyamide 6 (PA6) substrates, dual-responsive heat/humidity bilayer actuators are generated. The oriented PA6 guides the self-organization of the liquid crystal monomers into well-aligned, anisotropic liquid crystal networks. The bilayer responds to changes in the environmental relative humidity, resulting in bending of the actuator with the liquid crystal network inside the curvature. In contrast, in conditions of constant high humidity (80%RH), increasing the temperature triggers the liquid crystal network coating to bend the bilayer in the opposing direction. The dual-responsivity to changes in environmental humidity and temperature is examined in detail and discussed theoretically to elucidate the humidity-gated, temperature responsive properties revealing guidelines for fabricating anisotropic bilayer actuators.

Introduction

Advances in the field of stimuli-responsive actuators have led to the development of autonomously actuating systems triggered by environmental changes in pH, light, temperature and/or relative humidity.[1–6] The source of inspiration for these artificial actuators is found in nature, which features an impressive number of adaptive structures that respond to environmental changes.[7–9] Pine cones and feather grass, for example, liberate their seeds following different mechanisms: in dry conditions the pine cone scales open up and release their seeds, while members of the *Stipa* genus drill their seed into the soil at high humidity.[10–13] These shape changes have set standards for environmentally adaptive materials, showing promise for the fabrication of adaptive windows, facades and smart textiles for example.[14–18] Commodity polymers are appealing for fabricating these materials, since they are well-characterized, robust, and adding programmed responsivity will extend their range of applications.

In present literature, numerous stimuli-responsive commodity materials have been developed that respond to changes in environmental temperature or humidity.[19–23] These often multi-layer materials are commonly employed to obtain macroscopic bending, twisting or even rolling.[24–30] Yet, selecting the proper operating conditions is key to obtaining precise mechanical motions as temperature closely correlates to environmental relative humidity. This constraint is oftentimes circumvented by examining actuation under isothermal or constant humidity conditions.[31,32] The simultaneous interaction of both temperature and humidity on adaptive structures has been less explored, even though a better understanding of interconnected stimuli may lead to programmed environmentally adaptive materials.[33,34] Recent publications addressing the interplay of (photo)thermal and humidity reveal that a constant, high humidity is crucial in facilitating thermal response of the fabricated materials.[35,36]

Previously, we reported programmed helical twisting in humidity sensitive polyamide 6 (PA6) enabled by spray-coating of a chiral nematic liquid crystal (LC) that directed twisting.[37] In this work, we exploit the dual-responsivity of bilayer actuators based on the temperature sensitive liquid crystal network (LCN) and a humidity sensitive PA6 layer. We examine the anisotropic mechanical properties of the separate layers as simultaneous functions of temperature and humidity and the results serve as input for simple beam bending analysis. The detailed analysis reveals guidelines for fabricating anisotropic bilayer actuators towards robust, controlled stimulus sensitive films or fibers in pre-defined environmental conditions.

[a] *Laboratory of Stimuli-Responsive Functional Materials and Devices, Department of Chemical Engineering and Chemistry, Eindhoven University of Technology, P.O. Box 513, 5600 MB, Eindhoven, The Netherlands. E-mail: a.p.h.j.schenning@tue.nl*
[b] *Dutch Polymer Institute (DPI), P.O. Box 902, 5600 AX Eindhoven, The Netherlands*
[c] *Department of Mechanical Engineering, Materials Technology Institute, Eindhoven University of Technology, P.O. Box 513, 5600 MB Eindhoven, The Netherlands*
[d] *School of Engineering and Materials Science, Queen Mary University of London, Mile End Road, London E1 4NS, UK*

† Electronic supplementary information (ESI) available. See DOI: 10.1039/d0sm00030b

Experimental

Materials

The thermo-responsive LC mixture was prepared using 75 wt% of monomer 4-methoxybenzoic acid 4-(6-acryloyloxy-hexyloxy)phenyl ester (1, Synthon), 24 wt% covalent cross-linker 1,4-bis-[4-(6-acryloyloxyhexyloxy)benzoyloxy]-2-methylbenzene (2, Merck), and 1 wt% of photo-initiator phenylbis(2,4,6-trimethylbenzoyl)-phosphine oxide (3, Merck) dissolved in dichloromethane, stirred for an hour at 80 °C, and subsequently dried in a vacuum oven (80 °C, overnight). PA6 substrates were acquired from Goodfellow UK, and serve as the templates on which the LCs self-organize. All reagents were used as received.

Methods

Freestanding LCN films. Freestanding LCN films were produced by capillary force filling 30 × 30 mm^2, 70 μm gap glass cells prepared with anti-parallel rubbed polyimide alignment layers. The nematic phase was fixed by UV photo polymerization (20 mW cm^{-2} from an EXFO lamp for 600 seconds under nitrogen) at 45 °C followed by a post-curing step, 20 minutes at 130 °C. The solid LCN films were carefully removed from the cells.

LCN/PA6 bilayers. LCN/PA6-bilayer actuators were prepared by dissolving the LC mixture in a 1 : 5 wt ratio with xylene (Sigma Aldrich). An AMI 200 airbrush was employed to apply a ~4 μm LCN coating using N_2 as carrier gas at 1 bar on pre-dried PA6 substrates, and subsequently photo polymerized.

Shape morphing of 20 × 3 mm^2 bilayer films in response to changes in relative humidity (RH) and temperature was measured using a DataPhysics HGC 30 humidity chamber. Changing humidity levels was accomplished by using an integrated flow rate controller that fed dry and humid nitrogen gas. A second humidity sensor (Vaisala HM42 probe) was placed inside the chamber to verify the RH and temperature. Images were recorded with a smartphone camera and the images were analyzed using ImageJ open access software.

Characterization. Polarized optical micrographs were taken with a Leica DM2700 M to examine the alignment of the LCN films. The anisotropic mechanical properties of freestanding polymer films were measured on a TA instruments Q800 dynamic mechanical analyzer (DMA) equipped with a humidity chamber. Films of 10 × 5.3 mm^2 were mounted in a controlled environment. Elastic moduli (E) and $\tan\delta$ values were measured at a single frequency (1 Hz) and a 10 μm amplitude. Expansion coefficients were determined in controlled force experiments, where reversible changes in length were measured as a function of a thermal or humidity stimulus. Fourier transform infrared spectroscopy (FTIR) measurements were performed on a Varian 610 spectrophotometer. Calorimetric experiments were carried out on a TA Instruments DSC Q1000. Cross-sectional scanning electron micrographs were recorded under vacuum with a JSM-IT100 (JEOL).

Results and discussion

Bilayer actuators

The dual-responsive bilayer actuators were produced by combining a 15 μm PA6 layer with a 4 μm LCN coating (Fig. S1 and S2, ESI†).[37] The LCN consists of reactive mesogens (RMs) 1 and 2 mixed with photo-initiator 3 (Fig. S3, ESI†). The PA6 substrate was first cleaned with isopropanol, cut and taped to a 5 × 5 cm^2 glass slide. A flow of dry nitrogen removed water molecules from the PA6 prior to coating with a thin RM layer, which is then photo polymerized with UV-light to obtain a cross-linked network. Photo polymerization took place in the nematic phase (T < 58 °C). Bilayer strips of 20 × 3 mm^2 were cut from the larger films to study their deformation in response to temperature and humidity.

Self-alignment of the LCN is verified by polarized optical micrographs: a homogenous black image results when the alignment direction of the sample is parallel to one of the polarizers, and the characteristic bright image is obtained with the samples rotated 45° with respect to the polarizers (Fig. S4, ESI†). The LCN aligns planar at the PA6 interface and homeotropically at the air interface to minimize the surface free energy, an alignment that is commonly termed 'splay'. Polarized Fourier transform infrared spectroscopy was utilized to probe the optical anisotropy of the benzene rings and verify the splay molecular orientation (Fig. S5, ESI†).[24,38–40]

The LCN/PA6 bilayers are pre-bent at room temperature with the LCN on the outer diameter of the curvature – the inverse radius. This initial curvature results from the photo polymerization conditions of the LCN film: the LC is photo polymerized at 45 °C and ~0%RH before being exposed to lab conditions (20 °C and ~55%RH, respectively). The order of the LCN coating increases as it is cooled, and thus expands along the alignment direction (see Fig. 1), resulting in the PA6 being on the inside of the curvature.[1,40]

The pre-bent LCN/PA6 bilayer actuators were exposed to varying humidity levels and temperatures. At low humidity and room temperature (7.5%RH, 20 °C), upon gradually increasing the humidity level the humidity sensitive PA6 dominates the actuation process, inverting the curvature so the PA6 ends up on the outside at high (80%RH) humidity (Fig. 1).

At constant humidity (5%RH), the LCN is on the outer diameter of the curvature (Fig. 2A). Heating the bilayer did not show macroscopic actuation. At a thickness ratio of $d_{LCN}/d_{PA6} \sim 0.3$, this observation might be expected as the 4 μm thin LCN coating is unable to bend the much thicker 15 μm PA6 substrate. However, at high constant humidity (80%RH) thermal actuation

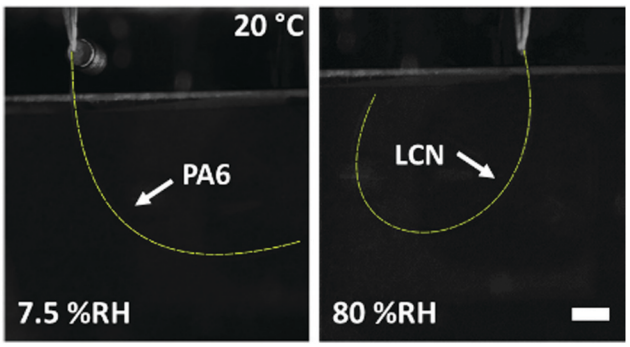

Fig. 1 Isothermal deformations (20 °C) of a 20 × 3 × 0.019 mm^3 LCN/PA6 actuator at two humidity levels, 7.5 and 80%RH. The scale bar equals 2 mm.

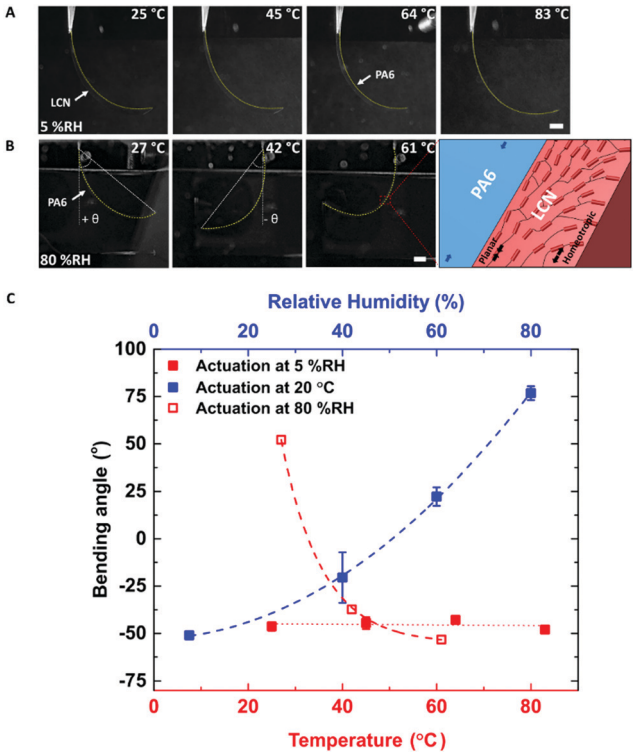

Fig. 2 The 20 × 3 × 0.019 mm^3 LCN/PA6 bilayer actuators exposed to different humidity and temperatures. (A) Thermal deformations of a bilayer strip in conditions of constant relative humidity (5%RH). The scale bar equals 2 mm. (B) Humidity-gated thermal actuation of the bilayer is displayed at 80%RH. The white dashed lines indicate positive or negative bending angles, θ. In the schematic illustration, the trilayer is illustrated in which the homeotropic and planar regions of the splay LCN and parallel PA6 layers are indicated, and each demonstrates different expansion characteristics upon heating. The scale bar equals 2 mm. (C) The bending angle of the bilayer actuators as a function of the applied stimuli depicted in the legend.

is observed (Fig. 2B), as PA6 binds significant amounts of moisture, revealing a humidity-gated thermal response of the bilayer.[41] This dual-responsiveness towards changes in surrounding humidity and/or temperature levels is depicted in Fig. 2C (with positive bending angle θ defined as PA6 being on the inner diameter of the curvature and negative with PA6 on the outer side). It should be noted that a bilayer actuator fabricated by spraying the liquid crystals and subsequent polymerization in the isotropic phase ($T \sim 80$ °C) did not actuate in water, demonstrating that the alignment of the liquid crystal is key to obtain humidity-gated temperature responsive actuation.

Singe layers

In order to understand the humidity-gated temperature response of the bilayer actuator, the individual mechanical properties of the LCN and PA6 layers were characterized. Freestanding LCN and PA6 films were studied with dynamic mechanical analysis (DMA). Films were cut both parallel and perpendicular to the orientation direction to measure storage moduli (E), damping (or energy dissipation), tan δ, and dimensional changes, strain (ε), as a function of both relative humidity and temperature. Heating both of the polymer films significantly affects the anisotropic mechanical properties, including the storage modulus E, tan δ, and the expansion, ε (see Fig. 3). The addition of thermal energy leads to a contraction along the director ($\varepsilon_x < 0$) and perpendicular expansion ($\varepsilon_y > 0$).[42] It is evident that the storage moduli of the component layers drop considerably after a threshold temperature: PA6 drops nearly ten-fold, and the LCN decreases by a factor of 100 (Fig. 3A). It is important to note that semi-crystalline PA6 has both crystalline and amorphous regions. The crystalline regions remain unaffected as the amorphous phase goes through the T_g and, therefore, restricts the decrease in PA6 modulus to the GPa range. In contrast, the LCN undergoes a transition from a glassy to a rubber-like material, explaining the steep decrease in elastic modulus. The tan δ peaks in Fig. 3B are typically used to detect molecular motion within a polymer, including the glassy to rubbery state transition.[43] The T_g of both LCN and PA6 are found to be centered at $T_{g,LCN} \sim 49$ °C and $T_{g,PA6} \sim 88$ °C. With increasing temperature, the polymers gain significant molecular mobility, meaning that there are less conformational restrictions, driving the network towards a random coil conformation, leading to contraction parallel (ε_x) and expansion perpendicular (ε_y) to the director orientation. Fig. 3C highlights the expansion coefficients of both polymers. Starting in the glassy state, strain values are small due to the restricted molecular motion of polymer chains.

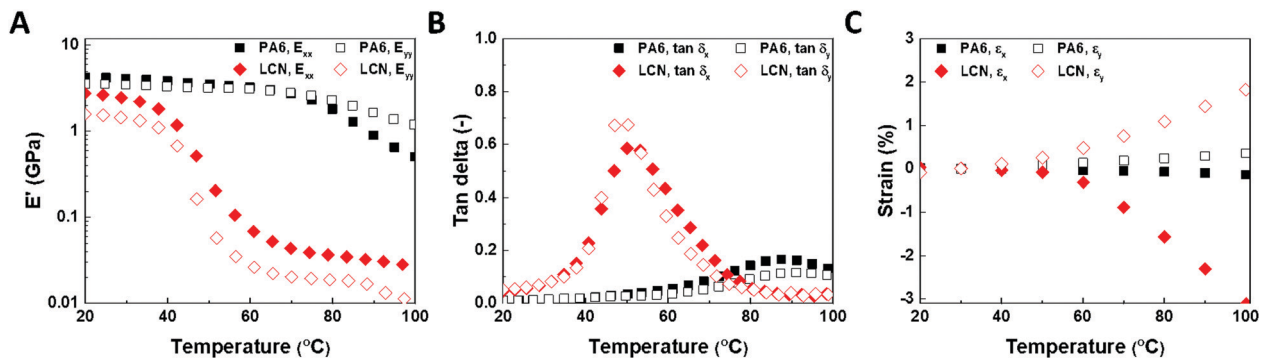

Fig. 3 (A) Storage moduli (E) in GPa of PA6 (black symbols) and the LCN (red symbols) measured parallel (filled symbols) and perpendicular (open symbols) to the LC alignment direction, plotted as a function of temperature. (B) The anisotropic tan delta (δ) values of both PA6 and LCN films. (C) Thermal expansion coefficients parallel (filled symbols) and perpendicular (open symbols) to the alignment direction.

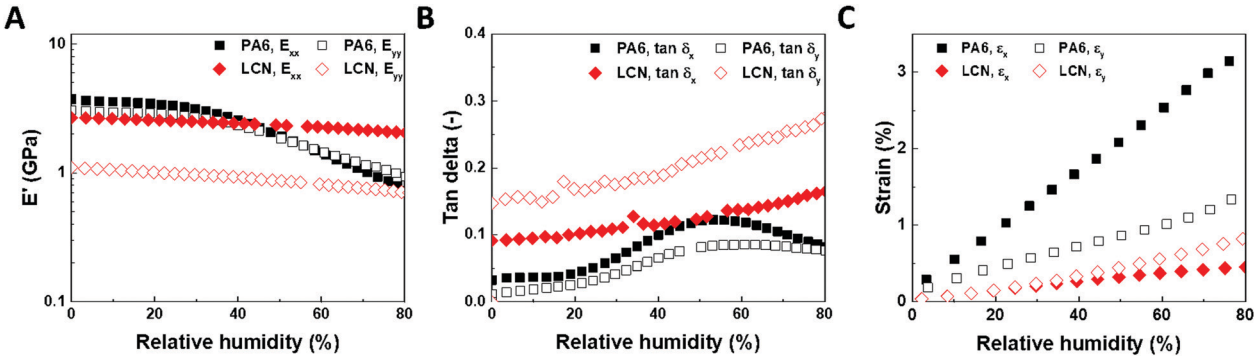

Fig. 4 (A) Storage moduli (E) of the hydrophilic PA6 (black symbols) and LCN (red symbols) films as a function of relative humidity. (B) The tan δ of PA6 and LCN freestanding films. (C) Anisotropic coefficients of humidity expansion given as strain-values (ε).

Around T_g, the polymer chains gain more segmental motion and expansion coefficients significantly increase in magnitude. The magnitude of contraction/expansion from oriented PA6 significantly diverges from that of the LCN as the methyl-substituent in C6M sterically hinders packing.[42,43]

The E, tan δ and ε-values for the individual LCN and PA6 freestanding films were also measured as a function of relative humidity, and displayed in Fig. 4. There are distinct differences between the responses of the LCN and PA6. The oriented PA6 has amorphous and crystalline blocks with polymer chains linked by intermolecular hydrogen bonds. In addition, free amide groups ab- and de-sorb water molecules, which in turn softens and expands/contracts the polymer matrix. The hydrophilic nature of PA6 is evident as E diminishes when moisture is absorbed at room temperature (RT).[37] Dried PA6 has E_{xx} = 4.3 GPa and E_{yy} = 3.5 GPa at room temperature, while at 80%RH E_{xx} and E_{yy} are reduced to 0.8 and 1.0 GPa, respectively. Fig. 4B shows that moisture absorption at room temperature results in a humidity induced T_g at ~50%RH. Effectively, humidity and temperature act equivalently in PA6, as at constant temperature the environmental humidity level induces a glass-to-rubber transition.[44,45] In contrast, in the LCN the moduli remain quite stable to changes of humidity; no T_g was detected from the tan δ *versus* relative humidity plot. Still, humidity does appear to influence the LCN (Fig. 4C).[46] Nevertheless, PA6 swells up to more than 3% of its initial length, significantly more than the LCN. In humid environments, water molecules penetrate into the amorphous regions of PA6 and hydrogen bond to the polymer backbone or occupy voids: the anisotropic swelling of oriented PA6 is mainly attributed to the distribution of alternating crystalline and amorphous regions along the orientation directions.[41]

In Fig. 5A–C, mechanical properties (E, tan δ and ε) are displayed as a function of temperature at 80%RH. Under these conditions, *i.e.* high humidity and at elevated temperature, PA6 is examined above its T_g, with little impact on the E and tan δ-values. Humidity and temperature can be used interchangeably to shift through T_g by changing the absorbed moisture content to access rubbery mechanical properties: the capacity to retain moisture by hydrogen bonding decreases modestly as the temperature increases.[47–49] These hydrogen bonded water molecules force apart crystalline blocks in PA6, impacting mechanical properties. Hence, a reduced capacity to bind water molecules increases polymer–polymer interactions, preserving a relatively high modulus of ~600 MPa at 80 °C and a larger thermal expansion parallel with respect to dry conditions. In contrast, the LCN layer is slightly swollen by the absorption of moisture and therefore tends to lower its moduli, E_{xx} and E_{yy}, as well as the T_g. Anisotropic thermal expansion is slightly amplified in a humid environment compared to dry conditions

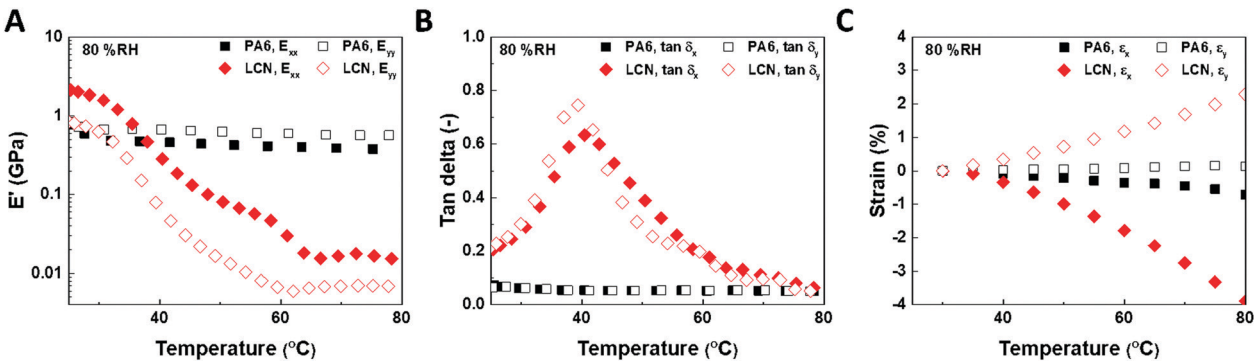

Fig. 5 (A) Storage moduli (E) in GPa of polyamide 6 (PA6, black symbols) and the LCN (red symbols) measured parallel (filled symbols) and perpendicular (open symbols) to the LC alignment direction, plotted as a function of temperature at 80%RH. (B) The anisotropic tan delta (δ) values of both PA6 and LCN films. (C) Thermal expansion coefficients parallel (filled symbols) and perpendicular (open symbols) to the alignment direction.

($\varepsilon_x \sim 4\%$ and $\varepsilon_y \sim 2.5\%$, resp.), which is believed to assist during humidity-gated actuation.

Working mechanism

With the detailed knowledge of physical characteristics of the individual layers, the interplay between the thermal and humidity responses of the bilayer films was examined using a classical approach to approximate curvature ($1/\rho$) changes in response to a stimulus described in Timoshenko's beam bending theory.[50] The theory factors in modulus ratio (n), thickness ratio (m), the total thickness (h) and the mismatch in expansion coefficients (ε) when a bilayer is submitted to environmental alterations.[4,8] Here, we interchangeably use heat or relative humidity as stimulus t, reflecting the experimental conditions that provoked the changes of curvature. At equilibrium conditions:

$$\frac{1}{\rho} = \frac{6 \cdot (\alpha_2 - \alpha_1) \cdot (t - t_0) \cdot (1+m)^2}{h \cdot \left(3 \cdot (1+m)^2 + (1 + m \cdot n) \cdot \left(m^2 + \frac{1}{m \cdot n}\right)\right)} \quad (1)$$

The theory is generally applicable only to isotropic systems, which is contrasting to the bilayer presented in this paper. However, in view of the high aspect ratio of the films, we assume material properties along the length of the strips dominate, *i.e.* in the x-direction (see Fig. 3–5). The analysis also assumes an initial flat strip that deflects when subjected to a stimulus, which differs from the experimentally observed pre-bend in Fig. 1 and 2. In these experiments/calculations only one parameter was varied, for example the humidity level was kept constant while the temperature was gradually increased. Table 1 lists the input values used in this analysis and the resultant outcomes. The modulus and expansion coefficients for the splay LCN are considered to be isotropic in nature; as the symmetric rod-like molecules gradually rotate out-of-plane (x,z-plane) the thermomechanical properties contribute equally in all directions:[42,43]

$$\varepsilon_{LCN} = \frac{\varepsilon_x + 2 \cdot \varepsilon_y}{3} \quad (2)$$

The trends correspond to the experimental observations: for example, at a constant 5%RH, the curvature scarcely changes when the temperature is raised to 80 °C. In contrast, the curvature increases dramatically when the humidity level is isothermally increased, whereas a temperature increase at 80%RH generates only a small curvature. The magnitude of deformations, defined as $1/\rho$ at equilibrium conditions, deviates from experimental observations, yet more detailed information regarding thermomechanical properties of the splay LCN could bridge the gap.[35,51] In essence, mesoscopic thermomechanical characterization of uniaxial LCN layers cannot completely describe humidity-gated deformations of the intrinsically complex splay aligned networks.[52,53] The gradual change in alignment likely requires *in situ* characterization of material properties combined with sophisticated finite element modelling to thoroughly predict humidity-gated deformations.[54–57] Nevertheless, analyzing the bilayer using the anisotropic mechanical properties of separate layers as input for the beam bending theory provides helpful information in designing future materials. In the LCN/PA6 bilayer actuators, thermal actuation of the LCN must compete with swelling of the hydrophilic PA6 base layer. The mismatch in expansion coefficients under different experimental conditions leads to differential bending of these bilayers. In the schematic illustration of Fig. 2B, the splay LCN can be subdivided into a homeotropic and planar layer that are 'stacked', effectively forming a 'trilayer' with the PA6.[40] In humidity-gated conditions, the PA6 layer in the pre-bent strip readily starts to desorb moisture when heated, leading to contraction of the bulk polymer. Synergistically, thermal expansion of the homeotropic region of the LCN should assist the macroscopic deformation towards PA6.[38,52] The final bending state assumed by the bilayer is the result of the competition between expansion coefficients for the two layers, the thermal expansion of the LCN countering the humidity-induced expansion of the PA6.

The exploration of anisotropic mechanical properties in oriented LCN and PA6 substrates has given new insights in the construction of multi-responsive bilayer actuators. Surprisingly, moisture does not deteriorate the storage moduli E_{xx} and E_{yy} of the LCN. PA6 is itself extremely sensitive to changes in humidity level. Thermally, the mechanical properties of both the LCN and PA6 diminish as they approach the glass transition regions at 49 °C and 88 °C, respectively. Both oriented materials contract in the orientation direction and expand orthogonally. Above 50 °C the storage moduli for both components diverge considerably, differing close to a factor 100 at elevated temperatures. In conditions of constant relative humidity (80%RH), thermal anisotropic material properties of the LCN and PA6 have been preserved: moduli are in the MPa range and thermal expansion of the LCN > PA6.

This work is a first step towards a well-tuned bilayer system, in which the relative thicknesses of the two components of the bilayer are carefully chosen; the combined material properties of thermal and humidity sensitivity could be exploited in applications such as stimuli-responsive garments, surgical tools or even soft robotics. A significant increase in the elongation at break (ε_b) of LCN films is found in the alignment direction of such composite materials (Fig. S6, ESI†).[25] To find application in devices, the magnitude of motions attained should be increased. One way to tune the bilayer properties is *via* selection of the RM composition. For example, preliminary work has found that LCN systems which consist only of diacrylates (the current system consists of only 25% diacrylates and 75% monoacrylates) swell up to only ε_x and ε_y values of 0.15% (Fig. S7, ESI†). Such changes in

Table 1 The deflection of a bilayer strip approximated using a classical beam bending theory under various experimental conditions, either at constant relative humidity or temperature. The input parameters of both liquid crystal network (LCN) and polyamide 6 (PA6) are defined at equilibrium conditions. The resulting curvature, $1/\rho$, is indicative for the deflection with respect to an initially flat strip

Stimulus	E_{LCN} (GPa)	E_{PA6} (GPa)	ε_{LCN} (%)	ε_{PA6} (%)	$1/\rho$ (mm^{-1})	Fig.
5 → 80%RH, at 20 °C	1.17	0.73	0.027	3.14	187.48	1
20 → 80 °C, at 5%RH	0.025	1.80	0.20	−0.071	−0.49	2A
20 → 60 °C, at 80%RH	0.016	0.40	0.19	−0.35	−2.76	2B

the composition result in a network with higher cross-link density, which translates to higher elastic moduli and T_g's, which could dramatically affect the bending characteristics of the bilayers. These type of LCN systems shall be discussed elsewhere.

Conclusions

Mechanically robust well-aligned bilayer actuators have been prepared by spray coating LCs on a stretched commodity polymer PA6 substrate. The RMs autonomously align onto the oriented PA6, and gradually rotate to homeotropic at the air interface, resulting in a splay alignment. Isothermally, the bilayer responds relatively strongly to changes in humidity, with extension by the PA6. In constant low RH (5%), the bilayer film curvature remains unchanged as temperature increases, whereas in more humid conditions (80%RH) the elastic moduli of PA6 is sufficiently lowered, resulting in humidity-gated deformation of the bilayer as the temperature increases.

The experimental observations were approximated using beam bending theory. Mechanical properties, determined with dynamic mechanical analysis, served as the input values to approximate the deflections of LCN/PA6 bilayer strips under various experimental conditions. We believe that by combining detailed knowledge of material properties and 1D beam bending theory, simple tools are provided to assist in the development of stimuli-responsive commodity polymers. As the fabrication method is not limited to PA6, other oriented commodity polymers could easily be functionalized by spraying liquid crystal coatings. Following similar procedures, careful evaluation of material properties in response to interconnected stimuli, such as temperature and humidity, could be exploited to extend their range of applications, for example in stimuli-responsive garments, surgical tools or even soft robotics.

Conflicts of interest

There are no conflicts to declare.

Acknowledgements

The work of Rob C. P. Verpaalen forms part of the research programme of DPI, project 731.015.502.

Notes and references

1 L. Ionov, *Soft Matter*, 2011, **7**, 6786–6791.
2 K. D. Harris, R. Cuypers, P. Scheibe, C. L. Van Oosten, C. W. M. Bastiaansen, J. Lub and D. J. Broer, *J. Mater. Chem.*, 2005, **15**, 5043–5048.
3 S. Iamsaard, S. J. Aßhoff, B. Matt, T. Kudernac, J. J. L. M. Cornelissen, S. P. Fletcher and N. Katsonis, *Nat. Chem.*, 2014, **6**, 229–235.
4 A. Agrawal, T. Yun, S. L. Pesek, W. G. Chapman and R. Verduzco, *Soft Matter*, 2014, **10**, 1411–1415.
5 J. Naciri, A. Srinivasan, H. Jeon, N. Nikolov, P. Keller and B. R. Ratna, *Macromolecules*, 2003, **36**, 8499–8505.
6 Y. Ma and J. Sun, *Chem. Mater.*, 2009, **21**, 898–902.
7 R. A. Sherry and C. Galen, *Plant, Cell Environ.*, 1998, **21**, 983–993.
8 A. Rafsanjani, V. Brulé, T. L. Western and D. Pasini, *Sci. Rep.*, 2015, **5**, 8064.
9 E. T. Nilsen, *Plant Physiol.*, 1987, **83**, 607–612.
10 E. Reyssat and L. Mahadevan, *J. R. Soc., Interface*, 2009, **6**, 951–957.
11 K. Song, S.-S. Chang and S. J. Lee, *Front. Life Sci.*, 2017, **10**, 38–47.
12 M. Aniszewska, *For. Res. Pap.*, 2013, **74**, 205–214.
13 A. Yanez, I. Desta, P. Commins, M. Magzoub and P. Naumov, *Adv. Biosyst.*, 2018, **2**, 1800007.
14 A. J. Boydston, B. Cao, A. Nelson, R. J. Ono, A. Saha, J. J. Schwartz and C. J. Thrasher, *J. Mater. Chem. A*, 2018, **6**, 20621–20645.
15 M. Bodaghi, A. R. Damanpack and W. H. Liao, *Smart Mater. Struct.*, 2018, **27**, 065010.
16 A. Saha, Y. Tanaka, Y. Han, C. M. W. Bastiaansen, D. J. Broer and R. P. Sijbesma, *Chem. Commun.*, 2012, **48**, 4579–4581.
17 J. Ter Schiphorst, S. Coleman, J. E. Stumpel, A. Ben Azouz, D. Diamond and A. P. H. J. Schenning, *Chem. Mater.*, 2015, **27**, 5925–5931.
18 N. A. Pattanashetti, G. B. Heggannavar and M. Y. Kariduraganavar, *Procedia Manuf.*, 2017, **12**, 263–279.
19 J. D. LeSar, N. M. Rao, N. M. Williams, J. P. Pantano, M. L. Ricci, L. S. Osher, V. J. Hetherington and J. S. Kawalec, *J. Am. Podiatr. Med. Assoc.*, 2016, **107**, 200–207.
20 L. Van Der Werff, I. L. Kyratzis, A. Robinson, R. Cranston, G. Peeters, M. O'Shea and L. Nichols, *J. Mater. Sci.*, 2013, **48**, 5005–5011.
21 K. D. Harris, C. W. M. Bastiaansen and D. J. Broer, *J. Microelectromech. Syst.*, 2007, **16**, 480–488.
22 Q. Zhu, Y. Jin, W. Wang, G. Sun and D. Wang, *ACS Appl. Mater. Interfaces*, 2019, **11**, 1440–1448.
23 M. Amjadi and M. Sitti, *Adv. Sci.*, 2018, **5**, 1800239.
24 M. Dai, O. T. Picot, J. M. N. Verjans, L. T. De Haan, A. P. H. J. Schenning, T. Peijs and C. W. M. Bastiaansen, *ACS Appl. Mater. Interfaces*, 2013, **5**, 4945–4950.
25 A. Ryabchun, F. Lancia, A.-D. Nguindjel and N. Katsonis, *Soft Matter*, 2017, **13**, 8070–8075.
26 J. A. H. P. Sol, A. R. Peeketi, N. Vyas, A. P. H. J. Schenning, R. K. Annabattula and M. G. Debije, *Chem. Commun.*, 2019, **55**, 1726–1729.
27 D. Han, Y. Liu, J. Ma, J. Mao, Z. Chen, Y. Zhang and H. Sun, *Adv. Mater. Technol.*, 2018, **3**, 1800258.
28 D.-D. Han, Y.-L. Zhang, J.-N. Ma, Y.-Q. Liu, B. Han and H.-B. Sun, *Adv. Mater.*, 2016, **28**, 8328–8343.
29 Y.-L. Zhang, J.-N. Ma, S. Liu, D.-D. Han, Y.-Q. Liu, Z.-D. Chen, J.-W. Mao and H.-B. Sun, *Nano Energy*, 2020, **68**, 104302.
30 W. Wang, Y. L. Zhang, B. Han, J. N. Ma, J. N. Wang, D. D. Han, Z. C. Ma and H. B. Sun, *Sens. Actuators, B*, 2019, **290**, 133–139.

31 H. Arazoe, D. Miyajima, K. Akaike, F. Araoka, E. Sato, T. Hikima, M. Kawamoto and T. Aida, *Nat. Mater.*, 2016, **15**, 1084–1089.
32 M. Chen, J. Frueh, D. Wang, X. Lin, H. Xie and Q. He, *Sci. Rep.*, 2017, **7**, 769.
33 K. Zhang, A. Geissler, M. Standhardt, S. Mehlhase, M. Gallei, L. Chen and C. Marie Thiele, *Sci. Rep.*, 2015, **5**, 11011.
34 M. Amjadi and M. Sitti, *ACS Nano*, 2016, **10**, 10202–10210.
35 E. P. A. Van Heeswijk, J. J. H. Kloos, N. Grossiord and A. P. H. J. Schenning, *J. Mater. Chem. A*, 2019, **7**, 6113–6119.
36 O. M. Wani, R. Verpaalen, H. Zeng, A. Priimagi and A. P. H. J. Schenning, *Adv. Mater.*, 2018, **1805985**, 1–6.
37 R. C. P. Verpaalen, M. G. Debije, C. W. M. Bastiaansen, H. Halilović, T. A. P. Engels and A. P. H. J. Schenning, *J. Mater. Chem. A*, 2018, **6**, 17724–17729.
38 C. L. Van Oosten, C. W. M. Bastiaansen and D. J. Broer, *Nat. Mater.*, 2009, **8**, 677–682.
39 E. Anglaret, M. Brunet, B. Desbat, P. Keller and T. Buffeteau, *Macromolecules*, 2005, **38**, 4799–4810.
40 G. N. Mol, K. D. Harris, C. W. M. Bastiaansen and D. J. Broer, *Adv. Funct. Mater.*, 2005, **15**, 1155–1159.
41 K. Inoue, S. Hoshino and U. Industries, *J. Polym. Sci., Part B: Polym. Phys.*, 1977, **15**, 1363–1378.
42 D. J. Broer and G. N. Mol, *Polym. Eng. Sci.*, 1991, **31**, 625–631.
43 R. A. M. Hikmet and D. J. Broer, *Polymer*, 1991, **32**, 1627–1632.
44 Y. Zheng and G. B. McKenna, *Macromolecules*, 2003, **36**, 2387–2396.
45 E. Parodi, G. W. M. Peters and L. E. Govaert, *J. Appl. Polym. Sci.*, 2018, **135**, 15–17.
46 Y. Liu, B. Xu, S. Sun, J. Wei, L. Wu and Y. Yu, *Adv. Mater.*, 2017, **29**, 1604792.
47 G. Baschek, G. Hartwig and F. Zahradnik, *Polymer*, 1999, **40**, 3433–3441.
48 A. Koshimo and T. Tagawa, *J. Appl. Polym. Sci.*, 1965, **9**, 45–54.
49 D. J. Skrovanek, S. E. Howe, P. C. Painter and M. M. Coleman, *Macromolecules*, 1985, **18**, 1676–1683.
50 S. Timoshenko, *J. Opt. Soc. Am.*, 1925, **11**, 233.
51 J. J. Wie, K. M. Lee, T. H. Ware and T. J. White, *Macromolecules*, 2015, **48**, 1087–1092.
52 C. D. Modes, M. Warner, C. L. van Oosten and D. Corbett, *Phys. Rev. E: Stat., Nonlinear, Soft Matter Phys.*, 2010, **82**, 041111.
53 M. Warner and E. M. Terentjev, *Liquid crystal elastomers*, 2003.
54 R. H. Pritchard, P. Lava, D. Debruyne and E. M. Terentjev, *Soft Matter*, 2013, **9**, 6037.
55 Y. Sawa, K. Urayama, T. Takigawa, V. Gimenez-Pinto, B. L. Mbanga, F. Ye, J. V. Selinger and R. L. B. Selinger, *Phys. Rev. E: Stat., Nonlinear, Soft Matter Phys.*, 2013, **88**, 022502.
56 L. Liu and P. R. Onck, *J. Mech. Phys. Solids*, 2019, **123**, 247–266.
57 W. Ren, P. J. McMullan and A. C. Griffin, *Phys. Status Solidi*, 2009, **246**, 2124–2130.